UC Davis

Title

Fine-tuning p53 activity by modulating the interaction between eukaryotic translation initiation factor eIF4E and RNA-binding protein RBM38

Permalink

Journal

ISSN

Authors

Sun, Wenqiang
Laubach, Kyra
Lucchessi, Christopher
et al.

Publication Date

DOI

Peer reviewed

Fine-tuning p53 activity by modulating the interaction between eukaryotic translation initiation factor eIF4E and RNA-binding protein RBM38

Wenqiang Sun,[1] Kyra Laubach,[1] Christopher Lucchessi,[1] Yanhong Zhang,[1] Mingyi Chen,[2] Jin Zhang,[1] and Xinbin Chen[1]

[1]Comparative Oncology Laboratory, School of Veterinary Medicine, School of Medicine, University of California at Davis, Davis, California 95616, USA; [2]Department of Pathology, University of Texas Southwestern Medical Center, Dallas, Texas 75390, USA

p53 is critical for tumor suppression but also elicits detrimental effects when aberrantly overexpressed. Thus, multiple regulators, including RNA-binding protein RBM38, are found to tightly control p53 expression. Interestingly, RBM38 is unique in that it can either suppress or enhance p53 mRNA translation via altered interaction with eIF4E potentially mediated by serine-195 (S195) in RBM38. Thus, multiple RBM38/eIF4E knock-in (KI) cell lines were generated to investigate the significance of eIF4E-RBM38 interaction in controlling p53 activity. We showed that KI of RBM38-S195D or -Y192C enhances, whereas KI of RBM38-S195K/R/L weakens, the binding of eIF4E to p53 mRNA and subsequently p53 expression. We also showed that KI of eIF4E-D202K weakens the interaction of eIF4E with RBM38 and thereby enhances p53 expression, suggesting that D202 in eIF4E interacts with S195 in RBM38. Moreover, we generated an Rbm38 S193D KI mouse model in which human-equivalent serine-193 is substituted with aspartic acid. We showed that S193D KI enhances p53-dependent cellular senescence and that S193D KI mice have a shortened life span and are prone to spontaneous tumors, chronic inflammation, and liver steatosis. Together, we provide in vivo evidence that the RBM38-eIF4E loop can be explored to fine-tune p53 expression for therapeutic development.

p53 tumor suppressor plays a pivotal role in maintaining genome integrity (Ko and Prives 1996). In response to cellular stress, p53 is activated and transcriptionally regulates a plethora of genes that are involved in multiple biological processes, including in cell cycle arrest, apoptosis, DNA damage repair, and senescence (Harms and Chen 2006). Due to its potent growth suppressive activity, p53 expression must be tightly controlled. Indeed, p53 expression is exquisitely regulated by several positive and negative regulators, often creating feedback loops (Harris and Levine 2005). For example, p53 forms a negative feedback loop with several E3 ligases including Mdm2, COP-1, and Pirh2 (Picksley and Lane 1993; Leng et al. 2003; Dornan et al. 2004), in that each of E3 ligases is induced by p53 and in turn lowers p53 activity. In addition, we showed previously that RNA-binding protein RBM38 is a target of p53 and can in turn repress p53 mRNA translation (Shu et al. 2006; Zhang et al. 2011). These positive and negative regulatory loops add more complexity to the p53 network. Thus, understanding of how p53 is regulated under normal and stress conditions, and the molecular mechanisms governing these regulatory processes, will lay a foundation to understand p53 biology and ultimately for the development of novel therapeutic strategies to target the p53 network for cancer management.

The RNA-binding protein RBM38 belongs to the RRM-containing RBP family. RBM38 has been implicated in multiple cellular processes, such as cell cycle arrest and differentiation, by regulating its downstream targets (Miyamoto et al. 2009; Zhang et al. 2010; Heinicke et al. 2013; Yin et al. 2013). Our group discovered that p53 transcriptionally activates RBM38, which in turn binds to p53

mRNA, interacts with eIF4E on the p53 mRNA, and represses p53 mRNA translation by blocking eIF4E from binding to the p53 m⁷G cap (Zhang et al. 2011). Thus, the mutual regulation between p53 and RBM38 forms a negative feedback loop (Zhang and Chen 2008). Interestingly, we also found that phosphorylation of RBM38 at Ser-195 by glycogen synthase kinase-3 (GSK3) facilitates the assembly of the eIF4F complex on p53 mRNA and, subsequently, enhances p53 mRNA translation, which is mediated by either promoting its interaction with eIF4G or disrupting the interaction between RBM38 and eIF4E (Zhang et al. 2013). Thus, RBM38 is a unique regulator of p53 as it can either enhance or inhibit p53 expression depending on the phosphorylation status of Ser-195. However, the critical residue in eIF4E that mediates interaction with Ser-195 in RBM38 has not yet been identified, and even less is known about the physiological significance of the RBM38-eIF4E loop in the p53 network.

In this study, we took advantage of CRISPR technology and generated multiple RBM38 and eIF4E knock-in (KI) cells lines. We found that the interaction between Ser-195 in RBM38 and aspartic acid (Asp) 202 in eIF4E is critical for modulating p53 mRNA translation. We also showed that two tumor-derived RBM38 mutants, Y192C and S195L, were capable of modulating p53 expression by altering their interaction with eIF4E. To further analyze the biological function of Ser-195 phosphorylation in RBM38, we generated a mutant *Rbm38* KI mouse model in which Ser-193 (equivalent to Ser-195 in human) is substituted with aspartic acid (S193D). We found that S193D KI mice had a shortened life span and were prone to spontaneous tumors, chronic inflammation, and liver steatosis.

Results

RBM38 S195D KI leads to growth suppression in a p53-dependent manner

We showed previously that RBM38 interacts with eIF4E through its C terminus (Zhang et al. 2013). In support of this, replica exchange molecular dynamics simulations (REMDS) showed that a potential binding pocket in eIF4E can interact with RBM38 protein through eight amino acids at its C terminus (Fig. 1A, left panel; Lucchesi et al. 2019). Based on the REMDS model, Ser-195 in RBM38 is predicted to interact with Asp-202 in eIF4E (Fig. 1A, right panel). Thus, to determine whether phosphorylation status of Ser-195 in RBM38 would modulate p53 expression in vivo, we generated multiple RBM38 KI cell lines in which Ser-195 in RBM38 is substituted with Asp (S195D, a phosphomimetic mutant). Two different RBM38-S195D KI HCT116 cell lines were generated. The first cell line was named *D/D* in that both alleles are S195D KI (Fig. 1B). The second cell line was named *D/−*, in which one *RBM38* allele is S195D KI and the other is null (Supplemental Fig. S1A). Interestingly, we found that the level of p53 protein, along with its bona fide target p21 (el-Deiry et al. 1993), was increased in both *D/D* and *D/*

− cells as compared with isogenic control cells (Fig. 1B; Supplemental Fig. S1A, p53 and p21 panels). Next, RNA-chip analysis was performed to examine whether S195D KI could alter the binding of eIF4E to p53 mRNA. We found that the binding of eIF4E to p53 mRNA was enhanced in both *D/D* and *D/−* cells as compared with isogenic control cells (Fig. 1C; Supplemental Fig. S1B, p53 panels, cf. lanes 5 and 6). As a negative control, S195D KI had no effect on the binding of eIF4E to actin mRNA (Fig. 1C; Supplemental Fig. S1B, actin panels, cf. lanes 5 and 6). Moreover, colony formation was performed and showed that the number of colonies was markedly reduced in *D/D* and *D/−* cells as compared with isogenic control cells (Fig. 1D; Supplemental Fig. S1C). Similarly, we also found that transient expression of S195D was able to enhance p53 and p21 expression and subsequently inhibit colony formation (Supplemental Fig. S1D,E), consistent with our previous report (Zhang et al. 2013). To verify this, isogenic control and *D/D* cells were used for three-dimensional (3D) spheroid culture. We found that the number of spheroids and cell viability were decreased in *D/D* cells as compared with isogenic control cells (Fig. 1E). Furthermore, to examine whether p53 is required for the suppressed cell proliferation in *D/D* and *D/−* cells, two p53 siRNAs along with a control siRNA were used for transient transfection into *D/ D* or *D/−* cells, followed by colony formation assay. As expected, the level of p53 protein was markedly decreased upon transfection with each p53 siRNA, together with a reduced expression of p21 (Fig. 1F; Supplemental Fig. S1F,H,J, p53 and p21 panels). Importantly, we found that the inhibited cell proliferation mediated by S195D KI was abrogated by knockdown of p53 in both *D/D* and *D/−* cells (Fig. 1G; Supplemental Fig. S1G,I,K). Together, these data suggest that RBM38 S195D KI leads to growth suppression in a p53-dependent manner.

RBM38 S193D KI mouse embryonic fibroblasts (MEFs) are prone to cellular senescence in a p53-dependent manner

To examine whether phosphorylation of Rbm38 at Ser-195 modulates p53 activity in vivo, an *Rbm38 S193D* KI mouse model in which human-equivalent serine-193 is substituted with aspartic acid was generated by a conventional embryonic stem cell-mediated homologous recombination strategy (Supplemental Fig. S2A,B). Next, a cohort of wild-type and *S193D/S193D* (*D/D*) MEFs was generated to examine whether *S193D* KI affects p53 expression. The *Rbm38⁻/⁻* MEFs were also used as a control since loss of *Rbm38* is known to enhance p53 expression (Zhang et al. 2011). We found that, like *Rbm38⁻/⁻* MEFs, *D/D* MEFs expressed higher levels of p53 protein than WT MEFs (Fig. 2A, p53 panel). Next, SA-β-gal staining was performed and showed that the percentage of SA-β-gal positive cells was much higher in *D/D* (56.5%) and *Rbm38⁻/⁻* (41.9%) MEFs than in WT MEFs (11.8%) (Fig. 2B). In line with this, the levels of p21 and p130, both of which are senescence markers (Campisi and di Fagagna 2007; Fiorentino et al. 2009), were increased in both *Rbm38⁻/⁻* and *D/D* MEFs as compared with WT MEFs
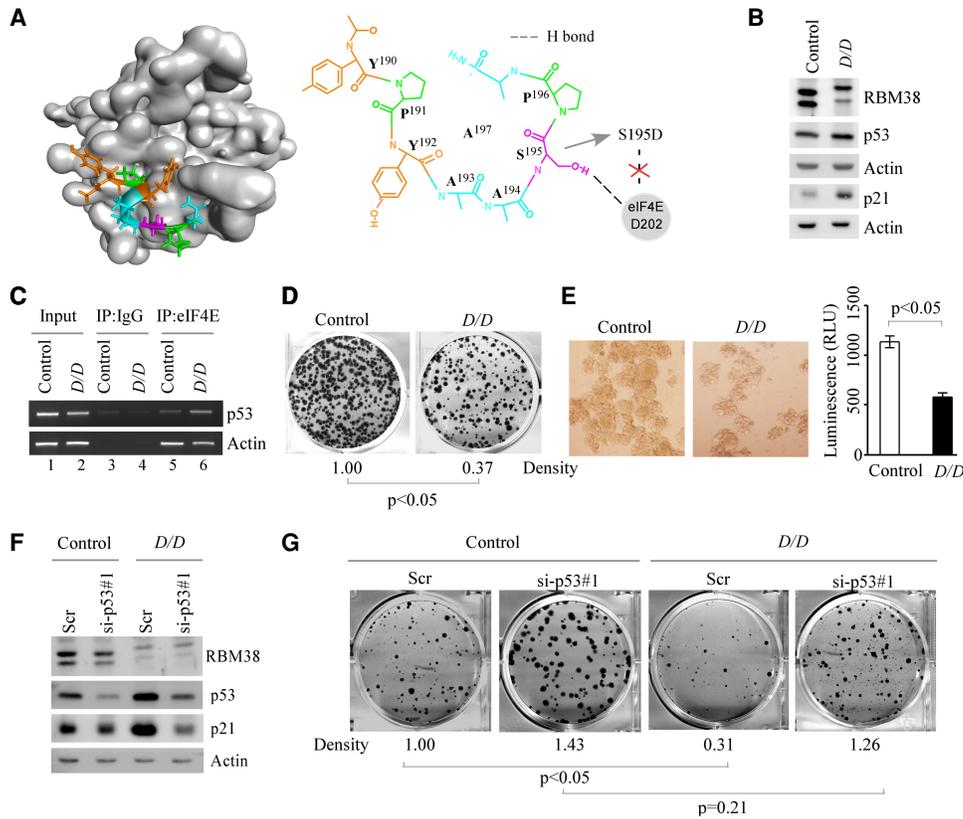
Figure 1. RBM38 S195D KI leads to growth suppression in a p53-dependent manner. (*A*, *left* panel) Representative docking image of eight-amino-acid fragment (amino acids 190–197) from Rbm38 to eIF4E based on replica exchange molecular dynamics simulations (REMDS). (*Right* panel) Predicted interaction between Ser-195 in RBM38 with Asp-202 in eIF4E. (*B*) The levels of RBM38, p53, and actin proteins were examined in isogenic control and *D/D* HCT116 cells. The first actin blot was the loading control for Rbm38 and p53 proteins whereas the second actin blot was for p21 protein. (*C*) An RNA-ChIP assay was performed to detect the binding of eIF4E to p53 mRNA in isogenic control and *D/D* HCT116 cells. The polysomal lysates from control and *D/D* HCT116 cells were immunoprecipitated with iso-type control IgG or anti-eIF4E antibody, and the protein–RNA complexes were brought down by protein A/G beads, followed by RT-PCR analysis to detect p53 or actin mRNA. (*D*) Colony formation assay was performed with isogenic control and *D/D* HCT116 cells. The rel-ative density was quantified and shown below each image. $P < 0.05$ indicates significance (Student's *t*-test). (*E*) Tumor spheroid assay was performed with isogenic control and *D/D* HCT116 cells. (*Left* panel) Representative images of spheroids from isogenic control and *D/D* cells. (*Right* panel) The viability of spheroids from isogenic control and *D/D* cells was analyzed by CellTiter-Glo assay. $P < 0.05$ indicates significance (Student's *t*-test). (*F*) Isogenic control and *D/D* cells were transfected with control or p53 siRNA #1 for 3 d and the levels of RBM38, p53, p21, and actin proteins were analyzed by Western blot analysis. (*G*) Colony formation assay was performed with isogenic control and *D/D* cells transfected with a control or p53 siRNA #1. The relative density was quantified and shown below each image. $P < 0.05$ indicates significance (Student's *t*-test).

(Fig. 2A, p21 and p130 panels). Similarly, the level of Cdnk2a (also known as p16^{INK4A}), another well-defined senescence marker (Krishnamurthy et al. 2004), was in-creased in *Rbm38*$^{-/-}$ and *D/D* MEFs as compared with WT MEFs (Fig. 2C, Cdkn2a panel). We also noticed that the level of Trp53 transcript was not altered in both *Rbm38*$^{-/-}$ and *D/D* MEFs (Fig. 2C, p53 panel), consistent with the notion that p53 is increased via mRNA transla-tion in these MEFs (Zhang et al. 2011). To verify that the increased p53 expression is responsible for the enhanced cellular senescence in *D/D* MEFs, we generated a cohort of *Trp53*$^{+/-}$ and *D/D*;*Trp53*$^{+/-}$ MEFs (Fig. 2D). Interesting-ly, we found that in the *Trp53*-heterozygosity background, *S193D* KI still led to enhanced p53 expression in MEFs (Fig. 2D). Moreover, despite the fact that the overall cellular

senescence was decreased in *Trp53*$^{+/-}$ MEFs, *D/D*;*Trp53*$^{+/-}$ MEFs (29.1%) were more prone to senescence than *Trp53*$^{+/-}$ MEFs (2%) (Fig. 2E). Consistent with this, we found that the levels of senescence markers, p21 (Fig. 2D) and Cdkn2a (Fig. 2F), were increased in *D/D*; *Trp53*$^{+/-}$ MEFs as compared with *Trp53*$^{+/-}$ MEFs. To verify that p53 is required for the enhanced cellular senescence in *D/D* MEFs, a cohort of *Trp53*$^{-/-}$ and *D/D*;*Trp53*$^{-/-}$ MEFs were generated (Fig. 2G). We found that both *Trp53*$^{-/-}$ and *D/D*;*Trp53*$^{-/-}$ MEFs were not prone to cellular senes-cence (<2%) (Fig. 2H). Moreover, the level of Cdkn2a tran-script was not altered between *Trp53*$^{-/-}$ and *D/D*;*Trp53*$^{-/-}$ MEFs (Fig. 2I). These data suggest that *S193D* KI increases p53 expression in MEFs and, subsequently, enhances cel-lular senescence in a p53-dependent manner.
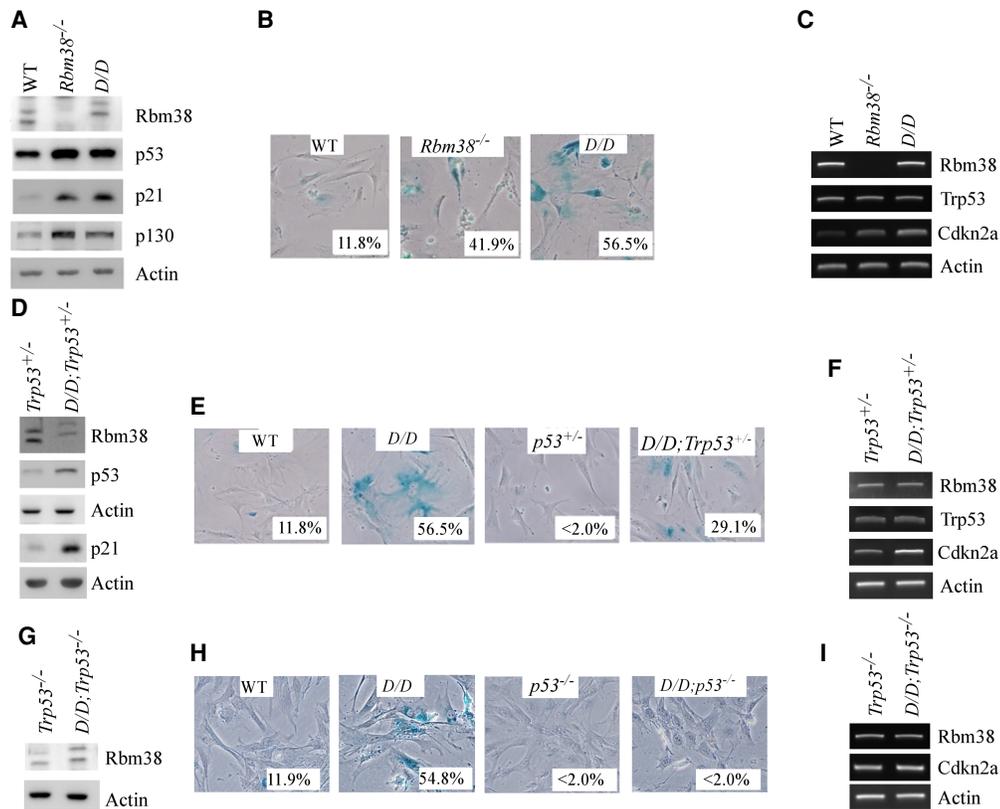
Figure 2. RBM38 S193D KI mouse embryonic fibroblasts (MEFs) are prone to cellular senescence in a p53-dependent manner. (*A*) The levels of Rbm38, p53, p21, p130, and actin proteins were examined in WT, $Rbm38^{-/-}$, and D/D MEFs. (*B*) SA-β-gal-staining was performed with WT, $Rbm38^{-/-}$, and D/D MEFs. The percentage of SA-β-gal-positive cells are shown inβ the *bottom right* corner in each image. (*C*) The levels of Rbm38, Trp53, Cdkn2a, and actin transcripts were examined in WT, $Rbm38^{-/-}$, and D/D MEFs. (*D*) The levels of Rbm38, p53, p21, and actin proteins were examined in $Trp53^{+/-}$, and $D/D;Trp53^{+/-}$ MEFs. The first actin was a loading control for Rbm38 and p53 and the second actin was a loading control for p21. (*E*) SA-β-gal-staining was performed with WT, D/D, $Trp53^{+/-}$, and $D/D;Trp53^{+/-}$ MEFs. The percentage of SA-β-gal-positive cells are shown in the *bottom right* corner of each image. (*F*) The levels of Rbm38, p53, Cdkn2a, and actin transcripts were examined in $Trp53^{+/-}$, and $D/D;Trp53^{+/-}$ MEFs. (*G*) The levels of Rbm38 and actin proteins were examined in $Trp53^{-/-}$ and $D/D;Trp53^{-/-}$ MEFs. (*H*) SA-β-gal-staining was performed with WT, D/D, $Trp53^{-/-}$, and $D/D;Trp53^{-/-}$ MEFs. The percentage of SA-β-gal-positive cells are shown in the *bottom right* corner in each image. (*I*) The levels of Rbm38, Cdkn2a, and actin transcripts were examined in $Trp53^{-/-}$ and $D/D;Trp53^{-/-}$ MEFs.

Knock-in of S195K or S195R decreases p53 expression by blocking the binding of eIF4E to p53 mRNA

Based on the REMDS model, Ser-195 in RBM38 is predicted to interact with Asp-202 in eIF4E (Fig. 1A). If Asp-202 in eIF4E truly interacts with Ser-195 in RBM38, substitution of Ser-195 by a positively charged amino acid, such as lysine or arginine, might lead to better interaction between RBM38 and eIF4E since KI of lysine or arginine not only disrupts phosphorylation of RBM38 but also forms hydrogen bound with the negatively charged D202 in eIF4E (Fig. 3A). To test this, we generated RBM38 KI cell lines in that Ser-195 is substituted by lysine (S195K) or arginine (S195R). One representative $K/+$ line, in which one allele is S195K KI and the is other wild type (Fig. 3B), and one representative R/R line, in which both alleles are S195R KI (Fig. 3C), were chosen for further analysis. We found that the levels of p53 and p21 proteins were decreased in both $K/+$ and R/R HCT116 cells as compared with isogen-ic control cells (Fig. 3B,C, p53 and p21 panels). Moreover, we showed that the binding of eIF4E to p53 mRNA was decreased in both $K/+$ and R/R HCT116 cells as compared with isogenic control cells (Fig. 3D,E, p53 panels, cf. lanes 5 and 6). Next, a colony formation assay was performed and showed that the number of colonies was markedly increased in $K/+$ and R/R cells (Fig. 3F,G). These data suggest that substitution of Ser-195 by lysine or arginine enhances its interaction with Asp-202 in eIF4E and thereby prevents eIF4E from binding to p53 mRNA, resulting in decreased p53 expression.

Tumor-derived RBM38 mutants, S195L and Y192C, exhibit distinct interactions with eIF4E and differentially modulate p53 expression

RBM38 has been found to be altered in several types of human cancer, such as lymphoma, acute myeloid leukemia,
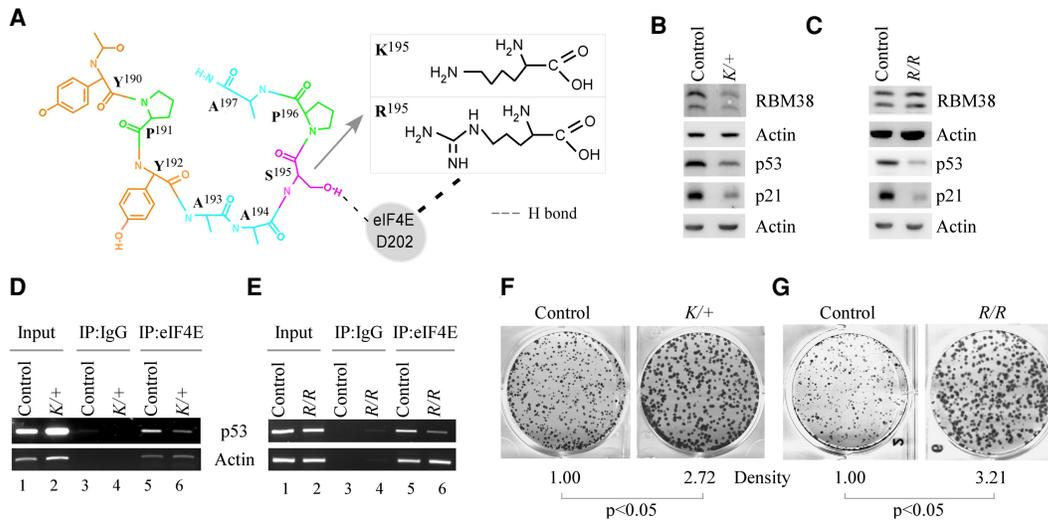
Figure 3. Knock-in of S195K or S195R decreases p53 expression by blocking the binding of eIF4E to p53 mRNA. (*A*) Schematic representation of the interactions between Asp-202 in eIF4E and Ser-195, S195K, or S195R in RBM38. (*B,C*) The levels of RBM38, p53, p21, and actin proteins were examined in an isogenic control (*B,C*), K/+ (*B*), or R/R (*C*) HCT116 cells. The first actin was a loading control for Rbm38 and the second actin was a loading control for p53 and p21. (*D,E*) RNA-ChIP analysis was performed with an isogenic control (*D,E*), K/+ (*D*), and R/R (*E*) cells. The polysomal lysates from control, K/+ and R/R cells were immunoprecipitated with isotype control IgG or anti-eIF4E antibody, and the protein-RNA complexes were brought down by protein A/G beads, followed by RT-PCR analysis. (*F,G*) A colony formation assay was performed with an isogenic control (*F,G*), K/+ (*F*), and R/R (*G*) cells. The relative density was quantified and is shown *below* each image. *P* < 0.05 indicates significance (Student's *t*-test).

and breast cancer (Zhang et al. 2011; Xue et al. 2014; Wampfler et al. 2016). Upon searching the COSMIC database (https://cancer.sanger.ac.uk/cosmic), we found several RBM38 mutations surrounding Ser-195 in cancer patients, including a Ser-195 to leucine mutation (S195L) (Fig. 4A). Since leucine is not a substrate for phosphorylation, we postulated that the S195L mutant may have a stronger interaction with eIF4E than wild-type RBM38 (Fig. 4A). To test this, we generated *S195L* KI HCT116 cell lines, and one representative *L/L* line, in which both alleles are S195L KI, was chosen for further analysis. We found that S195L KI leads to decreased expression of p53 and p21 in HCT116 cells (Fig. 4B, p53 and p21 panels). In support of this, the binding of eIF4E to p53 mRNA was decreased by S195L KI in *L/L* cells as compared with isogenic control cells (Fig. 4C, p53 panel, cf. lanes 5 and 6). Consequently, cell proliferation was enhanced in *L/L* cells as compared with isogenic control cells (Fig. 4D).

Tyr-192, which is three residues N-terminal of Ser-195, was found to be mutated to Cys (Y192C) in cancer. Tyrosine is a neutral amino acid, whereas cysteine is a smaller and hydrophobic amino acid. Based on the REMDS model, Tyr 192 is predicted to form hydrogen bonds with Thr-203 and Thr-204 in eIF4E (Fig. 4E). Thus, Y192C mutation in RBM38 would alter the local hydrogen bonding environment and subsequently affect RBM38's interaction with eIF4E. To test this, a Y192C expression vector was generated and then transiently transfected into HCT116 cells along with a control vector. We found that ectopic expression of Y192C led to increased expression of p53 and p21

(Supplemental Fig. S3A, p53 and p21 panels) and subsequently inhibited colony formation (Supplemental Fig. S3B). To verify this, RBM38 Y192C KI cell lines were generated and one C/+ line, in which one allele is Y192C KI and the other wild type (Fig. 4F), was chosen for further analysis. We found that the levels of p53 and p21 proteins were increased in *C/+* cells as compared with isogenic control cells (Fig. 4F, p53 and p21 panels). Consistently, the binding of eIF4E to p53 mRNA was increased by Y192C KI in *C/+* cells as compared with that by WT RBM38 in isogenic control cells (Fig. 4G, p53 panel, cf. lanes 5 and 6). Moreover, we found that the number of colonies was markedly decreased by Y192C KI in *C/+* cells as compared with isogenic control cells, presumably due to enhanced p53 expression (Fig. 4H). Furthermore, we showed that Y192C/+ cells were prone to cellular senescence along with increased expression of senescence markers (p130 and p21) as compared with isogenic control cells (Supplemental Fig. S3B–E).

Asp-202 is critical for eIF4E to interact with RBM38

The REMDS model predicts that Ser-195 in RBM38 interacts with Asp-202 in eIF4E (Fig. 1A). So far, we showed that substitution of Ser-195 with other amino acids alters the binding of eIF4E to p53 mRNA and subsequently modulates p53 expression (Figs. 1–4). Thus, it is worthwhile to determine whether Asp-202 in eIF4E is required for interaction with Ser-195 in RBM38. In this regard, we generated a mutant eIF4E-D202K in which the negatively charged Asp-202 was substituted with a positively charged lysine.
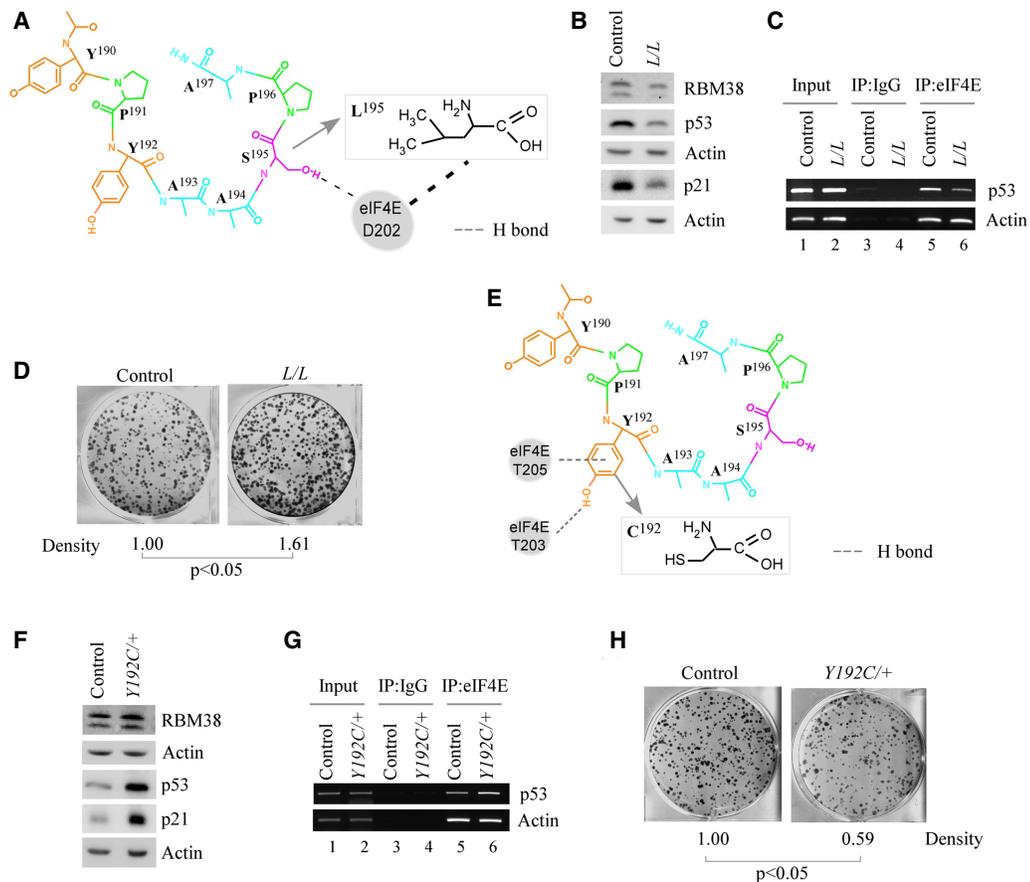
Figure 4. Tumor-derived RBM38 mutants, S195L and Y192C, exhibit distinct interactions with eIF4E and differentially modulate p53 expression. (*A*) Schematic representation of the interactions between Asp-202 in eIF4E and S195L or Y192C in RBM38. (*B*) The levels of RBM38, p53, p21, and actin proteins were analyzed in an isogenic control and *L/L* HCT116 cells. The first actin was a loading control for Rbm38 and p53 and the second actin was a loading control for p21. (*C*) RNA-ChIP analysis was performed to examine the binding of eIF4E to p53 mRNA in an isogenic control and *L/L* HCT116 cells. (*D*) A colony formation assay was performed with an isogenic control and *L/L* cells. The relative density was quantified and is shown *below* each image. $P < 0.05$ indicates significance (Student's *t*-test). (*E*) Schematic representation of how Tyr to Cys substitution at position 192 affects the interaction between RBM38 and eIF4E. (*F*) The levels of RBM38, p53, p21, and actin proteins were analyzed in an isogenic control and *Y192C/*+ HCT116 cells. The first actin was a loading control for Rbm38 and the second actin was a loading control for p53 and p21. (*G*) RNA-ChIP analysis was performed to examine the binding of eIF4E to p53 mRNA in an isogenic control and *Y192C/*+ HCT116 cells. (*H*) A colony formation assay was performed with an isogenic control and *Y192C/*+ cells. The relative density was quantified and is shown *below* each image. $P < 0.05$ indicates significance (Student's *t*-test).

First, we performed a cap-binding assay and found that, like wild-type eIF4E, mutant eIF4E-D202K was competent to bind to m⁷GTP-sepharose beads, suggesting that D202K mutation does not interfere with its cap-binding activity (Supplemental Fig. S4A). Next, a GST pulldown assay was performed to test the ability of eIF4E-D202K to interact with wild-type RBM38 or mutant RBM38-S195D (Fig. 5A). We showed that eIF4E-D202K had a weakened activity to interact with RBM38 as compared with wild-type eIF4E (Fig. 5B, eIF4E panel, cf. lanes 3 and 4). In contrast, eIF4E-D202K had a stronger interaction with RBM38-S195D than wild-type eIF4E (Fig. 5C, eIF4E panel, cf. lanes 3 and 4). These results suggest that D202K substitution restores the ability of eIF4E to interact with RBM38-S195D, consistent with the observation

that Asp-202 in eIF4E is required for the interaction with Ser-195 in RBM38 (Fig. 5A,B).

To further examine whether Asp-202 in eIF4E is required for interacting with Ser-195 in RBM38, mutant eIF4E KI HCT116 cell lines were generated (Fig. 5D,E). One representative *D202K/D202K* line, in which both alleles are D202K KI, and one representative *D202K/*− line, in which one eIF4E allele is D202K-KI and the other allele null, were chosen for further analysis. We found that both p53 and p21 were highly induced in *D202K/202K* and *D202K/*− cells compared with isogenic control cells (Fig. 5D,E). Interestingly, we were able to obtain a HCT116 cell line expressing a truncated eIF4E protein, called *ΔC17/*−, in which one allele is *eIF4E*-null and the other a deletion mutant *eIF4E* lacking the last 17
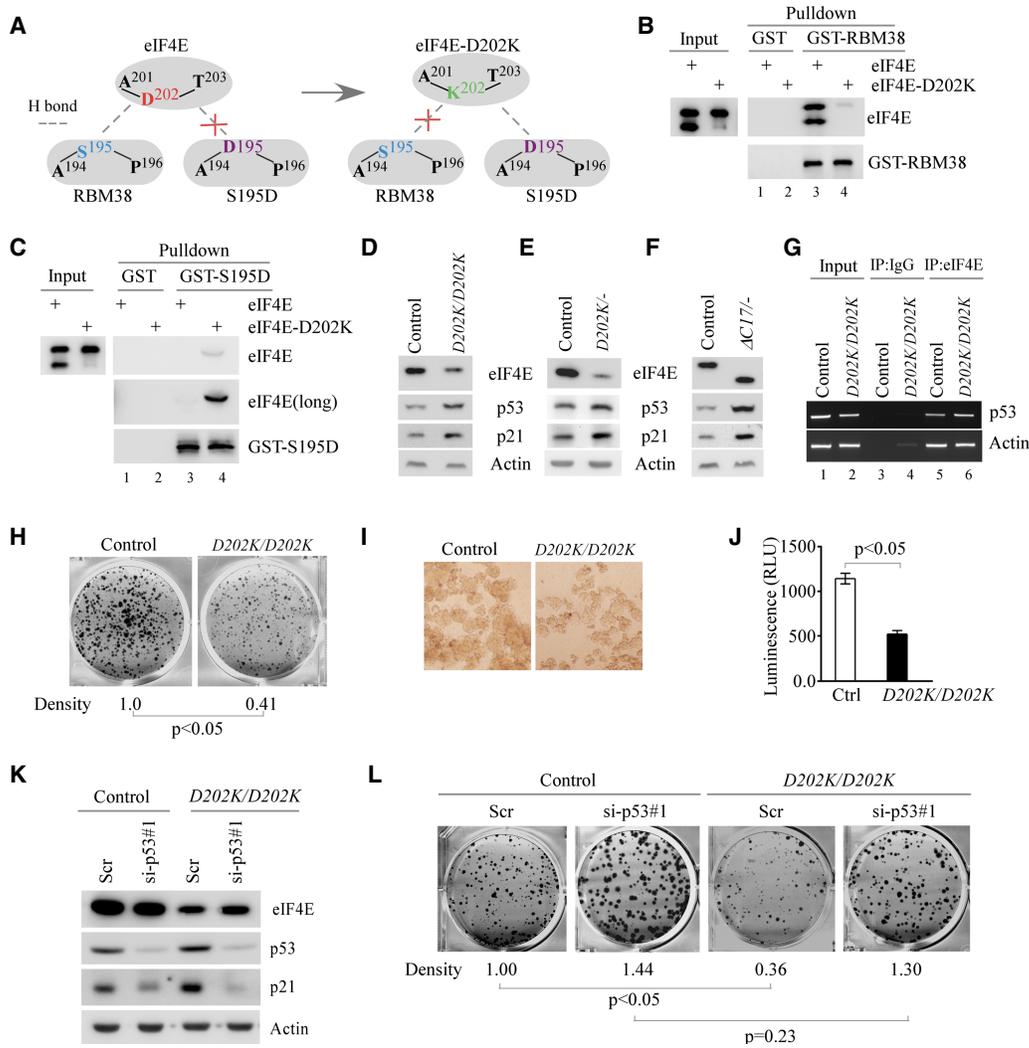
Figure 5. Asp-202 is critical for eIF4E to interact with RBM38. (*A*) Schematic representation of the interactions between eIF4E or eIF4E-D202K and wild-type RBM38 or RBM38-S195D. (*B*) A GST pull-down assay was performed using recombinant wild-type RBM38 with eIF4E or eIF4E-D202K. (*C*) A GST pull-down assay was performed using recombinant RBM38-S195D with eIF4E or eIF4E-D202K. (*D–F*) The levels of eIF4E, p53, p21, and actin proteins were analyzed in isogenic control (*D–F*), *D202K/D202K* (*D*), *D202K/–* (*E*), and *ΔC17/–* (*F*) cells. (*G*) An RNA-ChIP assay was performed with isogenic control and *D202K/D202K* cells to examine the binding of D202K KI to p53 mRNA. (*H*) A colony formation assay was performed with an isogenic control and *D202K/D202K* cells. The relative density was quantified and shown below each image. *P* < 0.05 indicates significance (Student's *t*-test). (*I*) Representative images of tumor spheroids formed by isogenic control and *D202K/D202K* HCT116 cells. (*J*) The viability of tumor spheroids from isogenic control and *D202K/D202K* HCT116 cells was analyzed by CellTiter-Glo assay. *P* < 0.05 indicates significance (Student's *t*-test). (*K*) Isogenic control and *D202K/D202K* cells were transfected with a control or p53 siRNA #1 for 3 d and the levels of eIF4E, p53, p21, and actin proteins were analyzed by Western blot analysis. (*L*) A colony formation assay was performed with HCT116 cells treated as in *K*. The relative density was quantified and shown below each image. *P* < 0.05 indicates significance (Student's *t*-test).

amino acids (amino acids 201–217). As expected, a smaller eIF4E protein was detected in *ΔC17/–* cells as compared with the full-length wild-type protein in isogenic control cells (Fig. 5F, eIF4E panel). We found that the levels of p53 and p21 proteins were increased in *ΔC17/–* cells as compared with that in isogenic control cells (Fig. 5F, p53 and p21 panels). These data suggest that the *ΔC17* mutant, which lacks Asp-202 and would not interact with RBM38, is able to increase p53 mRNA translation, as does eIF4E-D202K (Fig. 5D,E). Next,

RNA-chip analysis was performed and showed that the binding of eIF4E to the p53 mRNA was increased in *D202K/D202K* cells as compared with isogenic control cells (Fig. 5G, p53 panel, cf, lanes 5 and 6). Moreover, a colony formation assay was performed and showed that the number of colonies was reduced in *D202K/D202K* cells as compared with isogenic control cells (Fig. 5H). Similarly, a 3D organoid assay showed that the number and viability of tumor spheroids were decreased by KI of D202K (Fig. 5I,J). Furthermore, two p53 siRNAs were

used to confirm that p53 is required for growth suppression in *D202K/D202K* cells. We showed that the level of p53 protein was decreased by each p53 siRNA, but not scramble siRNA, which was accompanied with decreased expression of p21 (Fig. 5K; Supplemental Fig. S4B, p53 and p21 panels). Importantly, we found that the number of colonies reduced by *D202K* KI was abrogated upon knockdown of p53 in *D202K/D202K* cells (Fig. 5L; Supplemental Fig. S4C).

Rbm38-S193D *KI mice have a shortened life span and are prone to spontaneous tumors, chronic inflammation, and liver steatosis*

To understand the physiological activity of Ser-195 phosphorylation in vivo, $Rbm38^{S193D/S193D}$ (*D/D*) mice were generated (Supplemental Fig. S2B) and used to test p53 expression. We found that that the level of p53 protein was increased in the spleen tissue from a *D/D* mouse as com-

pared with that from a wild-type mouse (Fig. 6A), consistent with the observation that *S195D* KI increases p53 expression (Figs. 1, 2). Next, a cohort of WT, $Rbm38^{-/-}$, and *D/D* mice was generated and monitored for potential pathological abnormalities. We would like to mention that in order to minimize the number of animals used, the survival and tumor data for WT mice were adapted from two previous studies (Yang et al. 2017; Zhang et al. 2017). For $Rbm38^{-/-}$ mice, seven were generated for this study and 23 were generated previously (Zhang et al. 2014). All of the mice were derived from the same C57BL/6 background and maintained in the same animal facility. The median life span was 117 wk for WT mice, 101 wk for $Rbm38^{-/-}$ mice, and 101 wk for *D/D* mice (Fig. 6B; Supplemental Tables S1–S3). Like $Rbm38^{-/-}$ mice, *D/D* mice had a shortened life span as compared with WT mice ($P < 0.01$ by log rank test). However, the life span of *D/D* mice was not statistically different from that of $Rbm38^{-/-}$ mice ($P = 0.153$ by log rank test). Next,

Figure 6. Rbm38-S193D KI mice have a shortened life span and are prone to spontaneous tumors, chronic inflammation, and liver steatosis. (*A*) The levels of Rbm38, p53, p21, and actin proteins were analyzed in the spleen tissues from 4-wk-old WT and *D/D* mice. The first actin was a loading control for Rbm38 and p53, and the second actin was a loading control for p21. (*B*) Kaplan–Meier survival curves of WT ($n = 56$), $Rbm38^{-/-}$ ($n = 30$), and *D/D* ($n = 32$) mice. (*C*) Tumor spectrum and burden in WT ($n = 51$), $Rbm38^{-/-}$ ($n = 30$), and *D/D* ($n = 31$) mice. (*D*) The numbers and percentages of WT, $Rbm38^{-/-}$, and *D/D* mice with EMH. (*E*) The numbers and percentages of WT, $Rbm38^{-/-}$, and *D/D* mice with chronic inflammation in three or more organs. (*F*) The numbers and percentages of WT, $Rbm38^{-/-}$, and *D/D* mice with liver steatosis.

C The tumor spectra of WT, $Rbm38^{-/-}$ and *D/D* mice

Tumors	WT (n=51)	$Rbm38^{-/-}$ (n=30)	D/D (n=31)
DLBCL	6	0	8
TLBL	2	0	0
Unclassified LM	3	10	0
Histicytic sarcoma	1	1	1
Angiosarcoma	0	2	0
Spindle cell lipoma	0	0	2
Pyogenic granuloma	0	0	1
Adenocarcinoma	0	0	2
Skin adnexal tumor	0	0	1
Clonic adenoma	0	0	1
Hemangioma	0	1	0
Hepatoma	0	4	0
Total tumors	12	18	16
Tumor incidence/mice	11/51	15/30	14/31

LM: lymphoma; DLBCL: diffused large B cell lymphoma;
TLBL: T-Lymphoblastic lymphoma;

histopathological analysis was performed and showed that, like $Rbm38^{-/-}$ mice, D/D mice were prone to spontaneous tumors. The tumor incidence was significantly higher in D/D (14 out of 31, 45%) mice than in WT mice (11 out of 51, 21.5%; $P = 0.0291$ by Fisher's exact test) (Fig. 6C). Similarly, the tumor incidence of $Rbm38^{-/-}$ mice (15 out of 30, 50%) was significantly higher than that of WT mice ($P = 0.0131$ by Fisher's exact test), consistent with a previous report (Zhang et al. 2014). Notably, in addition to the common types of tumors, such as lymphomas, histiocytic sarcomas, and angiosarcomas, D/D and $Rbm38^{-/-}$ mice were prone to benign tumors. For example, D/D mice developed lipoma, granuloma, and adenoma, whereas $Rbm38^{-/-}$ mice developed hepatoma and hemangioma (Fig. 6C).

Histopathology analysis showed that, unlike $Rbm38^{-/-}$ mice, which exhibited splenomegaly and extramedullary hematopoiesis (Zhang et al. 2014), D/D mice were not prone to extramedullary hematopoiesis (Fig. 6D; Supplemental Tables S2, S3). Instead, D/D mice showed profound chronic inflammation in multiple organs, including kidney, lung, pancreas, and salivary gland (Supplemental Fig. S5A; Supplemental Table S3). We found that 67.7% of D/D mice (21 out of 31) exhibited inflammation in three or more organs as compared with 0% of wild-type mice and 33% of $Rbm38^{-/-}$ mice (10 out of 30) (Fig. 6E; Supplemental Tables S2–S3). In line with this, several proinflammatory cytokines, such as IL6, IL-17A, IL-1A, IL-2, and TNF-α, were increased in the livers of D/D mice as compared with WT mice (Supplemental Fig. S5B). Moreover, 38.7% D/D mice (12 out of 31) developed liver steatosis (Supplemental Fig. S5C), which was significantly higher than that in 5.9% of WT mice (three out of 51) and 13.3% of $Rbm38^{-/-}$ mice (four out of 30) (Fig. 6F; Supplemental Tables S1–S3). As several studies suggest that p53 promotes hepatic steatosis in mice (Derdak et al. 2013; Zhang et al. 2020), we asked whether p53 expression is increased in D/D mice with liver steatosis. To address this, p53 expression was examined in a D/D liver with steatosis along with a normal liver from age- and gender-matched wild-type mice. We found that p53 expression was increased in the D/D liver as compared with the WT liver (Supplemental Fig. S5D). Together, these data suggest that D/D mice had a shortened life span and were prone to spontaneous tumors, chronic inflammation, and liver steatosis.

Discussion

Our previous in vitro studies indicate that the phosphorylation status of Ser-195 in RBM38 acts as a switch to modulate p53 expression (Fig. 7; Zhang et al. 2013). To verify these findings in vivo, we used multiple biochemical and genetic approaches and showed that substitution of Ser-195 with Asp (S195D) enhances the binding of eIF4E to the p53 mRNA, leading to increased expression of p53, potentially via weakened interaction with eIF4E (Figs. 1, 2). In contrast, substitution of Ser-195 with lysine, arginine, or leucine (S195K, S195R, or S195L) decreases the binding of eIF4E to the p53 mRNA, leading to decreased p53 expression, potentially via enhanced interaction with eIF4E (Figs. 3, 4). Furthermore, we showed that substitution of Asp-202 with lysine in eIF4E weakens the ability of eIF4E to interact with RBM38 and leads to enhanced binding of eIF4E to p53 mRNA and increased p53 expression (Fig. 5). In line with this, we found that p53 expression was increased in ΔC17/– cells, which express a mutant eIF4E lacking the C-terminal 17 amino acids, including residue D202 (Fig. 5F). Together, these data and our early studies provide evidence for a model (Fig. 7) that a strong interaction between RBM38 with eIF4E would decrease, whereas a weak interaction would increase, the binding of eIF4E to p53 mRNA and subsequently p53 mRNA translation.

The REMDS model predicts that eight amino acids (amino acids 190–197; YPYAASPA; called Pep8) are involved in RBM38's interaction with eIF4E (Fig. 1A). Previously, we showed that Pep8 and Pep23, a 23-amino-acid peptide derived from eIF4E (amino acids 195–217), can disrupt the interaction between eIF4E and RBM38 and subsequently increase p53 expression (Lucchesi et al. 2019). Thus, the data from this study would provide an insight into how to modify Pep8 and Pep23 for stronger p53 induction. For example, since S195K and S195R showed a stronger interaction with eIF4E than wild-type RBM38 (Fig. 3), substitution of serine with lysine or arginine in Pep8 may further enhance its interaction with D202 in eIF4E and thereby elicit a stronger p53 induction. Our data also provide a foundation for developing small molecules that can disrupt RBM38-eIF4E interaction and thereby increase p53 expression for tumor suppression. Similarly, as S195-phosphorylated RBM38 is able to increase p53 expression (Zhang et al. 2013), we postulate that substitution of aspartic acid 202 with lysine in Pep23 (Pep23-
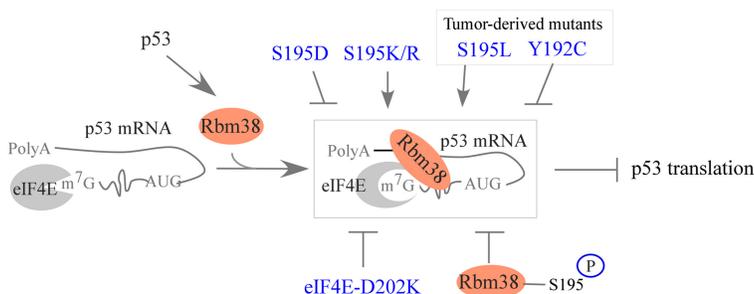
Figure 7. A model for how the RBM38-eIF4E complex modulates p53-dependent tumor suppression. A proposed model to elucidate how phosphorylation of RBM38 at serine-195 and various RBM38 and eIF4E mutants modulate the interaction between RBM38 and eIF4E and thereby regulate p53 mRNA translation.

D202K) would inhibit p53 expression as suggested by the observation that eIF4E-D202K has an enhanced interaction with RBM38-S195D and possibly S195-phosphorylated RBM38 (Fig. 5A,C). Inhibition of p53 expression is known to have therapeutic benefits, such as reduced toxicity during chemotherapy/radiotherapy (Komarov et al. 1999).

The COSMIC mutation database showed several RBM38 mutations surrounding Ser-195. In this study, we tested two tumor-derived RBM38 mutants, S195L and Y192C, for their abilities to regulate p53. We found that the S195L KI mutant inhibited p53 expression (Fig. 4B) whereas the Y192C KI mutant increased p53 expression (Fig. 4F). In support of this, we also found that the S195L KI mutant decreased, whereas the Y192C KI mutant enhanced, the binding of eIF4E to p53 mRNA (Fig. 4C,G). One interesting question is why RBM38 mutations elicit opposing effects on p53 expression in cancer. A potential answer to this question is that it may be related to p53 genetic status. We would like to mention that since Rbm38 regulates p53 mRNA translation (Zhang et al. 2011), it is not surprising that RBM38-Y192C would increase mutant p53 expression. Indeed, we found that p53 is mutated as p53-N239D in the same tumor with the RBM38-Y192C mutation, suggesting that tumor cells may select certain mutations for tumor progression. Additionally, we showed previously that loss of Rbm38 cooperates with mutant p53 to promote lymphomagenesis (Zhang et al. 2018). Several other RBM38 mutations, including A193T, A194T, and A197V, were detected in various tumors. Notably, residues A193, A194, and A197 are adjacent to Ser-195 and are predicted to modulate the interaction between RBM38 and eIF4E based on the REMDS model. These mutations are likely to alter the binding affinity of RBM38 to eIF4E. Unfortunately, due to the small numbers of these mutations found in human cancer samples, it is hard to correlate with p53 status at this moment. Nevertheless, further studies are needed to elucidate how these mutations would affect the RBM38-eIF4E interaction and, subsequently, p53-depedent tumor suppression.

With the novel *Rbm38-S193D* KI mouse model, we found that phosphormimetic Rbm38-S193D predisposes *D/D* mice to a shortened life span and spontaneous tumors, both of which are induced by loss of *Rbm38* in *Rbm38*$^{-/-}$ mice (Fig. 6B,C). Interestingly, *D/D* mice were also prone to chronic inflammation and liver steatosis (Fig. 6E,F). In contrast, unlike *Rbm38*$^{-/-}$ mice, D/D mice were not prone to EMH (Fig. 6D). These data suggest that the pathways being altered by *D/D* knock-in are similar to, but also distinct from, the ones altered by loss of *Rbm38*. Interestingly, one common phenotype is that p53 expression is enhanced in both *Rbm38*$^{-/-}$ and *D/D* mice while these mice were also prone to spontaneous tumors (Fig. 6A; Zhang et al. 2014). Thus, we postulate that the increased tumor incidence in these mice is likely to be p53-independent. For *Rbm38*$^{-/-}$ mice, the susceptibility to tumors is likely due to premature aging and splenomegaly upon loss of Rbm38 (Zhang et al. 2014). Since premature aging and splenomegaly were not or rarely observed in *D/D* mice, we hypothesize that the prevalence of the

chronic inflammation induced by Rbm38-S193D, which is often associated with SASP (senescence-associated secretory phenotype) and tends to promote tumor growth at a later stage (Coppé et al. 2010), is likely to counter the tumor suppressive activity by increased WT p53 expression, ultimately making D/D mice prone to spontaneous tumors. Alternatively, since p53 has been shown to enhance aging-associated chronic inflammation and progression of liver steatosis (Tomita et al. 2012; Derdak et al. 2013; Gudkov and Komarova 2016), it remains possible that increased p53 by Rbm38-S193D, possibly via premature senescence, may be responsible for chronic inflammation and, subsequently, spontaneous tumors exhibited in *D/D* mice. Nevertheless, these data suggest that increased expression of tumor suppressor p53 does not necessarily lead to tumor suppression and that other abnormalities, such as cellular senescence, chronic inflammation, and liver steatosis, may counter p53 tumor suppressive activity in a physiological setting. Thus, further studies are needed to address other biological functions of RBM38 Ser-195 phosphorylation and the biology of the p53-RBM38 regulatory loop. For example, does Ser-195 phosphorylation modulate p53-dependent tumor suppression in *D/D* mice with one or both null alleles of the *Trp53* gene? Does p53 play a role in chronic inflammation and liver steatosis in *D/D* mice? Does RBM38 Ser-195 phosphorylation correlate with p53 mutation and tumor progression in various human cancers?

Materials and methods

Reagents

Anti-actin (1:3000; sc-47778), anti-p130 (1:3000; sc-374521), anti-p21 (1:3000; sc-53870), and anti-eIF4E (1:2000; sc-9976) were purchased from Santa Cruz Biotechnology. Anti-p53 (1C12) (1:2000; 2524S) was purchased from Cell Signaling Technology. Anti-Rbm38 was custom-made as described previously (Shu et al. 2006). Scrambled siRNA (5′-GCAGUGUCUCCACGUACUA-3′) and *TP53* siRNA#1(5′-GAAAUUUGCGUGUGGAGUA-3′) and TP53 siRNA#2 (5′-GCACAGAGGAAGAGAAUCU-3′) were purchased from Dharmacon. For siRNA transfection, RNAiMax from Life Technologies was used according to the user's manual. Proteinase inhibitor cocktail was purchased from Sigma-Aldrich. Magnetic Protein A/G beads were purchased from MedChem. RiboLock RNase inhibitor and RevertAid first strand cDNA synthesis kit were purchased from Thermo Fisher.

Mice

Rbm38$^{-/-}$ mice (on a pure C57BL/6 background) were previously generated (Zhang et al. 2011). *Trp53*$^{+/-}$ mice (Jacks et al. 1994) were purchased from The Jackson Laboratory. *Rbm38-S193D* KI mice were generated by the University of California at Davis mouse biology program using traditional gene targeting techniques in embryonic stem cells. Specifically, the "knock-in cassette" consisted of LoxP sites that flanked the "WT exon 4 insert" and the neomycin (Neo) marker, followed by a "mutant exon 4 insert" with serine-193 replaced by aspartic acid. The knock-in cassette replaced the endogenous exon 4 through homologous recombination (HR). When bred with a Cre mouse

(Jackson Laboratories 003314), the WT exon 4 insert was deleted and the mutant exon 4 was transcribed and expressed (Supplemental Fig. S2A). The genotyping primers for the WT allele were forward primer 5′-CAGTACCCATATGCTGCCTCA-3′ and reverse primer 5′-AGGGCTGCAGAAGAAACTTG-3′. The genotyping primers for the S193D KI allele were forward primer 5′-CAGTACCCCTATGCTGCCGAC-3′ and the same reverse primer as for the WT allele. All animals and use protocols were approved by the University of California at Davis Institutional Animal Care and Use Committee.

MEF isolation

MEFs were isolated from 13.5-d-old embryos as described previously (Scoumanne et al. 2011) and cultured in Dulbecco's modified Eagle's medium (DMEM) supplemented with 10% fetal bovine serum (Invitrogen), 55 μM β-mercaptoethanol, and 1× nonessential amino acids (NEAA) solution (Cellgro). To isolate $Rbm38^{-/-}$ MEFs, $Rbm38^{+/-}$ mice were intercrossed. To isolate D/D MEFs, $D/+$ mice were bred with each other. To isolate $Trp53^{+/-}$, $Trp53^{+/-};D/D$, $Trp53^{-/-}$, and $Trp53^{-/-};D/D$ MEFs, $D/+$ mice were first bred with $Trp53^{+/-}$ mice to generate $Trp53^{+/-};D/+$ mice. Next, $Trp53^{+/-};D/+$ mice were bred with each other for MEF isolation.

Western blot analysis

Western blot procedures were as previously described (Dohn et al. 2001). Briefly, cell lysates were prepared with 2× SDS sample buffer. Proteins were separated in an 8%–12% SDS PAGE gel, transferred to nitrocellulose membrane, and incubated with indicated antibodies, followed by detection with enhanced chemiluminescence and visualized by VisionWorks LS software.

Plasmids

The pGEX vector expressing GST-tagged RBM38 was previously generated (Zhang et al. 2010). To generate the pGEX vector expressing GST-tagged Rbm38-S195D, two-step PCR reactions were performed. The first-step PCR reaction was performed to separately amplify two PCR fragments by using Rbm38 cDNA as a template. Fragment #1 was amplified with forward primer 5′-AAAGAATTCATGCTGCTGCAGCCCGCGCC-3′ and reverse primer 5′-CGTGGCAGGGTCGGCGGCGTATGGG-3′. Fragment #2 was amplified with forward primer 5′-CCGCCGACCCTGCCACGGCTGCCAG-3′ and reverse primer 5′-AAACTCGAGTCACTGCATCCTGTCAGGCTG-3′. The second-step PCR was performed by using fragments #1 and #2 as templates together with the forward primer for fragment #1 and the reverse primer for fragment #2. These PCR products were inserted into the pGEX vector through EcoRI and XhoI sites and confirmed by sequencing. To generate pTXB1-eIF4E, PCR product was amplified by using full-length eIF4E cDNA as a template with forward primer 5′-GGTGGTCATATGGCGACTGTCGAACCGG AAACC-3′ and reverse primer 5′-GGTGGTTGCTCTTCC GCAAACAACAAACCTATTTTTAGTGGTGGAG-3′. To generate pTXB1-eIF4E-D202K, two-step PCR reactions were performed. The first-step PCR reaction was performed to separately amplify two PCR fragments by using eIF4E cDNA as a template. Fragment #1 was amplified with the same forward primer of eIF4E and reverse primer 5′-GTAGCTGTCTTT GCGTGGGACTG-3′. Fragment #2 was amplified with forward primer 5′-CAGTCCCACGCAAAGACAGCTAC-3′ and the same reverse primer of eIF4E. The second-step PCR was amplified using fragments #1 and #2 as templated with the forward and re-

verse primers of eIF4E. The PCR product of eIF4E and eIF4E-D202K was cloned into the pTXB1 vector through NdeI and SapI sites.

To generate plasmids containing various homologous recombination templates (S195D/K/R/L and Y192C mutant), an 800-bp DNA fragment was amplified using HCT116 cell genomic DNA as a template with forward primer 5′-CCGCCGTCGTGGC TTCAAACT-3′ and reverse primer 5′-GAATGCCCGAGC GGTCTTCG-3′. This DNA fragment was then cloned into the pGEMT vector and used as a template for generating Rbm38- KI HR templates using two-step PCR. To generate the HR template containing S195D KI, the first-step PCR was to separately amplify two DNA fragments #1 and #2. The primers to amplify fragment #1 were forward primer 5′-CCGCCGTCGTGGCTTCAAACT-3′ and reverse primer 5′-CAGCAGTGGCAGGATCCGCGGCGTA TGGGTAC-3′. The primers for fragment #2 were forward primer 5′-CGCGGATCCTGCCACTGCTGCCAGCTTCGTG-3′ and reverse primer 5′-GAATGCCCGAGCGGTCTTCG-3′. The second-step PCR was amplified using fragments #1 and #2 as templates with the forward primer of fragment #1 and the reverse primer of fragment #2. The PCR products were then cloned into the pGEMT vector and confirmed by sequencing. To generate the HR template with S195K KI, the same strategy was used except with the reverse primer 5′-GGCAGGCTTGGCGGCAT ATGGGTACTGGTCATAGGTG-3′ used for fragment #1 and forward primer 5′-CATATGCCGCCAAGCCTGCCACGGC TGCCAGCTTC-3′ used for fragment #2. To generate the HR template with S195R KI, the same strategy was used except with reverse primer 5′-GGCAGGCCTGGCGGCATATGGGT ACTGGTCATAGGTG-3′ used for fragment #1 and forward primer 5′-CATATGCCGCCAGGCCTGCCACGGCTGCCAGC TTC-3′ used for fragment #2. To generate the HR template with S195L KI, the same strategy was used except with reverse primer 5′-GGCAGGCCGTGGCAGGGAGTGCGGCATATGGGTACTG ATCATATG-3′ used for fragment #1 and forward primer 5′-CAT ATGATCAGTACCCATATGCCGCACTCCCTGCCACGGCT GCC-3′ used for fragment #2. To generate the HR template with Y192C KI, the same strategy was used except with reverse primer 5′-CTGTAGCCCACGAACGACGCAGCCGTGGCAGGCGAC GCGGCACATGGGTACTGATCATATGTGGCCGG-3′ used for fragment #1 and forward primer 5′-CCGGCCACATATGAT CAGTACCCATGTGCCGCGTCGCCTGCCACGGCTGCGTC GTTCGTGGGCTACAG-3′ used for fragment #2. To generate the HR template with eIF4E-D202K KI, a 1200-bp DNA fragment was amplified using HCT116 cell genomic DNA with forward primer 5′-TATTTGCTAGGGTTCAGACGTGAAATG-3′ and reverse primer 5′-CAGCCATCAGCAAGAGTACAGCAAAG-3′. The PCR product was then cloned into the pGEMT vector and used as a template for the eIF4E-D202K HR template. The first step was to amplify fragments #1 and #2. The primers for fragment #1 were forward primer 5′-GGGACTGTCCTTAC TTTGTTCACTGTTG-3′ and reverse primer 5′-CAAATCTAT TTTTAGTGGTGGAGCCTGATTTAGTAGCTGTCTTTGCG TGAGA-3′. The primers to amplify fragment #2 were forward primer 5′-TCTCACGCAAAGACAGCTACTAAATCAGGCTC CACCACTAAAAATAGATTTG-3′ and reverse primer 5′-CAG CCATCAGCAAGAGTACAGCAAAG-3′. The second-step PCR was amplified using fragments #1 and #2 as template with the forward primer for fragment #1 and the reverse primer for fragment #2. The PCR products were then cloned into the pGEMT vector.

Cell culture and cell line generation

HCT116 cells were cultured in DMEM supplemented with 10% fetal bovine serum. HCT116 KI cell lines were generated using

CRISPR-Cas9 technology along with an asymmetric donor DNA as previously described (Richardson et al. 2016). Briefly, HCT116 cells were cotransfected with a single-stranded oligodeoxynucleotide (ssODN) together with sgRNA, followed by puromycin selection for 3 wk. Individual clones were picked and confirmed by sequencing. It should be mentioned that the sequence of ssODN should be the same as the target strand to achieve the best HDR efficiency as previous described (Richardson et al. 2016). To generate a vector expressing a single-guide RNA (sgRNA), two 25-nt oligos were annealed and then cloned into pSpCas9(BB) (Ran et al. 2013). Two sgRNAs were used for RBM38 KI cell line generation: The sequence for sgRNA#1 was 5′-GCGAGGCGGCGTATGGGTAC-3′, and the sequence for sgRNA#2 was 5′-GGCGTATGGGTACTGGTCAT-3′. Two sgRNAs were used for eIF4E KI cell line generation: The sequence for sgRNA#1 was 5′-CTTAGTAGCTGTGTCTGCGT-3′, and the sequence for sgRNA#2 was 5′-GCGGCTCCACCACTAA AAAT-3′. To generate various RBM38 KI ssODNs, asymmetrical PCR was performed as previously described (Pagratis 1996). Briefly, the first round of PCR was to amplify double-stranded DNAs using various RBM38 KI templates (S195D/K/R/L and Y192C) with forward primer 5′-AACCATTCAAGATTTT TATTTTTGCACCAG-3′ and reverse primer 5′-GAATGCCC GAGCGGTCTTCG-3′. The products from the first-round PCR were then used as a template for a second-round PCR with only a forward primer. To generate eIF4E KI ssODNs, the same strategy was used. The double-stranded DNAs from the first round of PCR were amplified with forward primer 5′-GGGACTGTC CTTACTTTGTTCACTGTTG-3′ and reverse primer 5′-CAGC CATCAGCAAGAGTACAGCAAAG-3′. To generate ssODNs, either the forward or reverse primer from the first round PCR was used for asymmetrical PCR.

GST pull-down assay

To purify recombinant eIF4E and eIF4E-D202K protein, pTXB1-eIF4E or pTXB1-eIF4E-D202K was transformed into bacteria BL21, which were induced with 0.1 mmol/L IPTG for 4 h. Bacteria lysates were incubated with chitin beads rocking at 4°C for 1 h, washed with column buffer (500 mM NaCl), and the recombinant protein was eluted in an elution buffer. For GST pull-down assay, pGEX-Rbm38 or pGEX-Rbm38-S195D was transformed into bacteria BL21 and induced with 0.1 mmol/L IPTG for 4 h. Bacteria lysates were then incubated with GST beads for 2 h at 4°C, washed with PBST, and resuspended in cold PBS. The RBM38 or RBM38-S195D bead slurry was incubated with purified recombinant eIF4E or eIF4E-D202K overnight at 4°C and washed three times with PBST. The samples were then eluted with 60 µL of 1× SDS-loading buffer for Western blot analysis.

Tumor spheroid culture

HCT116 cells (~2500) were washed five times with PBS, resuspended in MammoCult (Stemcell) media, and then mixed with Matrigel (Corning). The ratio for Mammocult versuss Matrigel was 3:4 with a total volume of 15 µL. Each mixture was pipetted in triplicate around the rim of each well in a 96-well plate and incubated 15 min at 37°C, followed by adding100 µL of Mammo-Cult media. Six days later, 50 µL of dispase (5 mg/mL; Stem Cell Technologies) was added to each well at 37°C and cell viability was measured by using a CellTiter-Glo 3D cell viability assay kit (Promega) according to the manufacturer's guidelines.

RT-PCR analysis

Total RNAs were isolated with Trizol reagent (Invitrogen Life Technologies), followed by cDNA synthesis using RevertAid first

strand cDNA synthesis kit (Thermo Fisher Scientific). The PCR program used for amplification was (1) 5 min at 94°C, (2) 45 sec at 94°C, (3) 45 sec at 60°C, (4) 45 sec at 72°C, and (5) 10 min at 72°C. From steps 2 to 4, the cycle was repeated 22–35 times depending on the transcripts amplified. The primers used to amplify mouse *ACTIN* was forward primer 5′-TCCATCATGAAGTGT GACGT-3′ and reverse primer 5′-TGATCCACATCTGCTGG AAG-3′. The primers used to amplify mouse *Rbm38* were forward primer 5′-GACGCATCGCTCAGAAAGT-3′ and reverse primer 5′-GAGGAGTCAGCCCGTAGGT-3′. The primers used to amplify mouse Trp53 were forward primer 5′-CTTCCTCCAG AAGATATCCTG-3′ and reverse primer 5′-GCCATAGTTG CCCTGGTAAG-3′. The primers to amplify mouse Cdkn2a were forward primer 5′-ATGGAGTCCGCTGCAGACAGAC TG-3′ and reverse primer 5′-GAAGGTAGTGGGGTCCTCGCA GTTC-3′.

RNA-ChIP assay

RNA chromatin immunoprecipitation (RNA-ChIP) was performed as described (Peritz et al. 2006). Briefly, cells extracts were prepared with immunoprecipitation buffer (10 mM HEPES at pH 7.0, 100 mM KCl, 5 mM MgCl$_2$, 0.5% NP40, 1 mM DTT) and then incubated with 2 µg of anti-eIF4E or an isotype control IgG overnight at 4°C. The RNA-protein immunocomplexes were brought down by protein A/G beads. RT-PCR analysis was carried out to determine the levels of *TP53* and *Actin* transcripts. The primers to amplify human *Actin* were forward primer 5′-CTGAAGTACCCCATCGAGCACGGCA-3′ and reverse primer 5′-GGATAGCACAGCCTGGATAGCAACG-3′. The primers to amplify human *TP53* were forward primer 5′-GACCGGCGCACAGAGGAAGAGAATC-3′ and reverse primer 5′-GAGTTTTTTATGGCGGGAGGTAGAC-3′.

Colony formation

HCT116 cells and their derivatives (~1000 per well) were seeded in triplicate in a six-well plate and then maintained in fresh medium for 2 wk. The clones were fixed using methanol/glacial acetic acid (7:1) followed by crystal violet staining. The color density of clones was scanned and analyzed using ImageJ software with the ColonyArea plugin installed as previously described (Guzmán et al. 2014).

SA-β-gal staining

The senescence assay was performed as described previously (Qian et al. 2008). Briefly, primary MEFs at passage 5 were seeded into a six-well plate and maintained in fresh medium for 72 h. Cells were then washed with 1× phosphate-buffered saline and fixed with a fixing solution (2% formaldehyde, 0.2% glutaraldehyde in PBS) for 15 min at room temperature, followed with fresh β-gal staining solution (1 mg/mL 5-bromo-4-chloro-3-indolyl-b-d-galactopyranoside, 40 mM citric acid/sodium phosphate at pH 6.0, 5 mM potassium ferrocyanide, 5 mM potassium ferricyanide, 150 mM NaCl, 2 mM MgCl$_2$) overnight at 37°C without CO$_2$.

Histological analysis

Mouse tissues were fixed in neutral buffered formalin for 18 h and embedded in paraffin blocks. Tissue blocks were sectioned and stained with hematoxylin and eosin.

Statistical analysis

The log rank test was used for Kaplan–Meier survival analysis. Two-tailed Student's *t*-tests was performed for the statistical analysis of the SA-*β*-gal staining assay, RT-PCR, and colony formation assay. Values of $P < 0.05$ were considered significant.

Competing interest statement

The authors declare no competing interests.

References

Campisi J, di Fagagna FD. 2007. Cellular senescence: when bad things happen to good cells. *Nat Rev Mol Cell Bio* **8:** 729–740. doi:10.1038/nrm2233

Coppé JP, Desprez PY, Krtolica A, Campisi J. 2010. The senescence-associated secretory phenotype: the dark side of tumor suppression. *Annu Rev Pathol-Mech* **5:** 99–118. doi:10.1146/annurev-pathol-121808-102144

Derdak Z, Villegas KA, Harb R, Wu AM, Sousa A, Wands JR. 2013. Inhibition of p53 attenuates steatosis and liver injury in a mouse model of non-alcoholic fatty liver disease. *J Hepatol* **58:** 785–791. doi:10.1016/j.jhep.2012.11.042

Dohn M, Zhang S, Chen X. 2001. P63α and ΔNp63α can induce cell cycle arrest and apoptosis and differentially regulate p53 target genes. *Oncogene* **20:** 3193–3205. doi:10.1038/sj.onc.1204427

Dornan D, Wertz I, Shimizu H, Arnott D, Frantz GD, Dowd P, O'Rourke K, Koeppen H, Dixit VM. 2004. The ubiquitin ligase COP1 is a critical negative regulator of p53. *Nature* **429:** 86–92. doi:10.1038/nature02514

el-Deiry WS, Tokino T, Velculescu VE, Levy DB, Parsons R, Trent JM, Lin D, Mercer WE, Kinzler KW, Vogelstein B. 1993. WAF1, a potential mediator of p53 tumor suppression. *Cell* **75:** 817–825. doi:10.1016/0092-8674(93)90500-P

Fiorentino FP, Symonds CE, Macaluso M, Giordano A. 2009. Senescence and p130/Rbl2: a new beginning to the end. *Cell Res* **19:** 1044–1051. doi:10.1038/cr.2009.96

Gudkov AV, Komarova EA. 2016. P53 and the carcinogenicity of chronic inflammation. *Cold Spring Harb Perspect Med* **6:** a026161. doi:10.1101/cshperspect.a026161

Guzmán C, Bagga M, Kaur A, Westermarck J, Abankwa D. 2014. ColonyArea: an ImageJ plugin to automatically quantify colony formation in clonogenic assays. *PLoS One* **9:** e92444. doi:10.1371/journal.pone.0092444

Harms KL, Chen X. 2006. The functional domains in p53 family proteins exhibit both common and distinct properties. *Cell Death Differ* **13:** 890–897. doi:10.1038/sj.cdd.4401904

Harris SL, Levine AJ. 2005. The p53 pathway: positive and negative feedback loops. *Oncogene* **24:** 2899–2908. doi:10.1038/sj.onc.1208615

Heinicke LA, Nabet B, Shen S, Jiang P, van Zalen S, Cieply B, Russell JE, Xing Y, Carstens RP. 2013. The RNA binding protein RBM38 (RNPC1) regulates splicing during late erythroid differentiation. *PLoS One* **8:** e78031. doi:10.1371/journal.pone.0078031

Jacks T, Remington L, Williams BO, Schmitt EM, Halachmi S, Bronson RT, Weinberg RA. 1994. Tumor spectrum analysis in *p53*-mutant mice. *Curr Biol* **4:** 1–7. doi:10.1016/S0960-9822(00)00002-6

Ko LJ, Prives C. 1996. p53: puzzle and paradigm. *Genes Dev* **10:** 1054–1072. doi:10.1101/gad.10.9.1054

Komarov PG, Komarova EA, Kondratov RV, Christov-Tselkov K, Coon JS, Chernov MV, Gudkov AV. 1999. A chemical inhibitor of p53 that protects mice from the side effects of cancer therapy. *Science* **285:** 1733–1737. doi:10.1126/science.285.5434.1733

Krishnamurthy J, Torrice C, Ramsey MR, Kovalev GI, Al-Regaiey K, Su L, Sharpless NE. 2004. Ink4a/Arf expression is a biomarker of aging. *J Clin Invest* **114:** 1299–1307. doi:10.1172/JCI22475

Leng RP, Lin Y, Ma W, Wu H, Lemmers B, Chung S, Parant JM, Lozano G, Hakem R, Benchimol S. 2003. Pirh2, a p53-induced ubiquitin-protein ligase, promotes p53 degradation. *Cell* **112:** 779–791. doi:10.1016/S0092-8674(03)00193-4

Lucchesi CA, Zhang J, Ma B, Chen M, Chen X. 2019. Disruption of the Rbm38-eIF4E complex with a synthetic peptide Pep8 increases p53 expression. *Cancer Res* **79:** 807–818. doi:10.1158/0008-5472.CAN-18-2209

Miyamoto S, Hidaka K, Jin D, Morisaki T. 2009. RNA-binding proteins Rbm38 and Rbm24 regulate myogenic differentiation via p21-dependent and -independent regulatory pathways. *Genes Cells* **14:** 1241–1252. doi:10.1111/j.1365-2443.2009.01347.x

Pagratis NC. 1996. Rapid preparation of single stranded DNA from PCR products by streptavidin induced electrophoretic mobility shift. *Nucleic Acids Res* **24:** 3645–3646. doi:10.1093/nar/24.18.3645

Peritz T, Zeng F, Kannanayakal TJ, Kilk K, Eiríksdóttir E, Langel U, Eberwine J. 2006. Immunoprecipitation of mRNA-protein complexes. *Nat Protoc* **1:** 577–580. doi:10.1038/nprot.2006.82

Picksley SM, Lane DP. 1993. The p53-mdm2 autoregulatory feedback loop: a paradigm for the regulation of growth control by p53? *Bioessays* **15:** 689–690. doi:10.1002/bies.950151008

Qian Y, Zhang J, Yan B, Chen X. 2008. DEC1, a basic helix-loop-helix transcription factor and a novel target gene of the p53 family, mediates p53-dependent premature senescence. *Journal of Biological Chemistry* **283:** 2896–2905. doi:10.1074/jbc.M708624200

Ran FA, Hsu PD, Wright J, Agarwala V, Scott DA, Zhang F. 2013. Genome engineering using the CRISPR-Cas9 system. *Nat Protoc* **8:** 2281–2308. doi:10.1038/nprot.2013.143

Richardson CD, Ray GJ, DeWitt MA, Curie GL, Corn JE. 2016. Enhancing homology-directed genome editing by catalytically active and inactive CRISPR-Cas9 using asymmetric donor DNA. *Nat Biotechnol* **34:** 339–344. doi:10.1038/nbt.3481

Scoumanne A, Cho SJ, Zhang J, Chen XB. 2011. The cyclin-dependent kinase inhibitor p21 is regulated by RNA-binding protein PCBP4 via mRNA stability. *Nucleic Acids Res* **39:** 213–224. doi:10.1093/nar/gkq778

Shu L, Yan W, Chen X. 2006. RNPC1, an RNA-binding protein and a target of the p53 family, is required for maintaining the stability of the basal and stress-induced p21 transcript. *Genes Dev* **20:** 2961–2972. doi:10.1101/gad.1463306

Tomita K, Teratani T, Suzuki T, Oshikawa T, Yokoyama H, Shimamura K, Nishiyama K, Mataki N, Irie R, Minamino T, et al. 2012. P53/p66Shc-mediated signaling contributes to the progression of non-alcoholic steatohepatitis in humans and mice. *J Hepatol* **57:** 837–843. doi:10.1016/j.jhep.2012.05.013

Wampfler J, Federzoni EA, Torbett BE, Fey MF, Tschan MP. 2016. The RNA binding proteins RBM38 and DND1 are repressed in AML and have a novel function in APL differentiation. *Leuk Res* **41:** 96–102. doi:10.1016/j.leukres.2015.12.006

Xue JQ, Xia TS, Liang XQ, Zhou W, Cheng L, Shi L, Wang Y, Ding Q. 2014. RNA-binding protein RNPC1: acting as a tumor suppressor in breast cancer. *BMC Cancer* **14:** 322. doi:10.1186/1471-2407-14-322

Yang HJ, Zhang J, Yan WS, Cho SJ, Lucchesi C, Chen MY, Huang EC, Scoumanne A, Zhang WC, Chen XB. 2017. Ninjurin 1 has two opposing functions in tumorigenesis in a p53-dependent manner. *Proc Natl Acad Sci* **114:** 11500–11505. doi:10.1073/pnas.1711814114

Yin T, Cho SJ, Chen X. 2013. RNPC1, an RNA-binding protein and a p53 target, regulates macrophage inhibitory cytokine-1 (MIC-1) expression through mRNA stability. *J Biol Chem* **288:** 23680–23686. doi:10.1074/jbc.M113.480186

Zhang J, Chen X. 2008. Posttranscriptional regulation of p53 and its targets by RNA-binding proteins. *Curr Mol Med* **8:** 845–849. doi:10.2174/156652408786733748

Zhang J, Cho SJ, Chen XB. 2010. RNPC1, an RNA-binding protein and a target of the p53 family, regulates p63 expression through mRNA stability. *Proc Natl Acad Sci* **107:** 9614–9619. doi:10.1073/pnas.0912594107

Zhang J, Cho SJ, Shu L, Yan W, Guerrero T, Kent M, Skorupski K, Chen H, Chen X. 2011. Translational repression of p53 by RNPC1, a p53 target overexpressed in lymphomas. *Genes Dev* **25:** 1528–1543. doi:10.1101/gad.2069311

Zhang M, Zhang J, Chen X, Cho SJ, Chen X. 2013. Glycogen synthase kinase 3 promotes p53 mRNA translation via phosphorylation of RNPC1. *Genes Dev* **27:** 2246–2258. doi:10.1101/gad.221739.113

Zhang J, Xu ES, Ren C, Yan WS, Zhang M, Chen MY, Cardiff RD, Imai DM, Wisner E, Chen XB. 2014. Mice deficient in Rbm38, a target of the p53 family, are susceptible to accelerated aging and spontaneous tumors. *Proc Natl Acad Sci* **111:** 18637–18642. doi:10.1073/pnas.1415607112

Zhang YH, Qian YJ, Zhang J, Yan WS, Jung YS, Chen MY, Huang E, Lloyd K, Duan YY, Wang J, et al. 2017. Ferredoxin reductase is critical for p53-dependent tumor suppression via iron regulatory protein 2. *Gene Dev* **31:** 1243–1256. doi:10.1101/gad.299388.117

Zhang J, Yang HJ, Zhang YH, Chen MY, Chen XB. 2018. Loss of Rbm38 cooperates with mutant p53 to promote lymphomagenesis through downregulation of Pten. *Cancer Res* **78**.

Zhang X, Lin Y, Lin S, Li C, Gao J, Feng Z, Wang J, Zhang J, Zhang H, Zhang Y, et al. 2020. Silencing of functional p53 attenuates NAFLD by promoting HMGB1-related autophagy induction. *Hepatol Int* **14:** 828–841. doi:10.1007/s12072-020-10068-4